Applied Catalysis B: Environmental 158–159 (2014) 258–268

Contents lists available at ScienceDirect

Applied Catalysis B: Environmental

journal homepage: www.elsevier.com/locate/apcatb

Focus on the modified $Ce_xZr_{1-x}O_2$ with the rigid benzene-muti-carboxylate ligands and its catalysis in oxidation of NO

Wei Cai[a,b], Qin Zhong[a,b,*], Wei Zhao[a,b], Yunfei Bu[a,b]

[a] School of Chemical Engineering, Nanjing University of Science and Technology, Nanjing 210094, China
[b] Nanjing AIREP Environmental Protection Technology Co., Ltd, Nanjing 210091, China

ARTICLE INFO

Article history:
Received 31 October 2013
Received in revised form 11 April 2014
Accepted 14 April 2014
Available online 21 April 2014

Keywords:
Benzene-muti-carboxylate ligand
Ceria–zirconia solid solution
Selective catalytic oxidation
NO

ABSTRACT

A modified $Cr/Ce_xZr_{1-x}O_2$ with the rigid benzene-muti-carboxylate ligands are prepared and studied on the oxidation of NO. These catalysts were investigated in detail by means of X-ray diffraction (XRD), High resolution transmission electron microscope (HR-TEM), Brunauer–Emmett–Teller (BET) surface area analysis, Ultra violet–visible diffuse reflectance spectroscopy (UV–vis DRS), X-ray photoelectron spectroscopy (XPS), $NO(O_2)$ Temperature-programmed desorption ($NO(O_2)$-TPD) and in-situ diffuse reflectance infrared Fourier transform spectroscopy (DRIFTS). The results demonstrated that the catalysts prepared with cinnamic acid as precipitant showed a higher surface area, a lower band gap and a stronger ability to adsorb reactant gas. Otherwise, the ligands such as terephthalic acid and trimesic acid were unfavorable for the synthesis of $Ce_xZr_{1-x}O_2$ due to the long distance between the carboxyl groups. Furthermore, the π–π conjugated effect of the cinnamic acid balanced the charge in the precursor of the catalysts prepared with cinnamic acid, thus leading to their band gaps lower than that of other catalysts after calcinations. The catalytic performance over the catalysts prepared with cinnamic acid exhibited the highest NO conversion, and the preparation with one-pot method was simpler. Moreover, the catalyst prepared with one-pot method showed well ability to resist the poison effect of H_2O and SO_2, which was due to the large surface area. Finally, while combined the XPS analysis, in-situ DRIFTS demonstrated that the adsorbed NO interacted with the adsorbed O_2 to generate NO_2, and the adsorption and activation O_2 was the key factor.

1. Introduction

The emission of nitrogen oxides (NO_x) originated from the combustion of most fuels causing ozone depletion, photochemical smog and the acid deposition, are hazardous to the environment and human health [1]. Selective catalytic oxidation (SCO) method plays a decisive role in those main technologies of NO_x decrease, such as NO_x storage and reduction (NSR) [2–4], continuously regenerating trap (CRT) [5] and selective catalytic reduction (SCR) [6–10]. This technology is a possible way to conduct SCR at low cost, and can avoid possible corrosion of ammonia in SCR. The key of SCO is NO to NO_2 and if the ratio of NO/NO_x equals to 60%, the removal effect will be the optimum [9,11]. Ceria–zirconia solid solutions ($Ce_xZr_{1-x}O_2$) were prepared on oxidation reaction by many researchers for its excellent abilities of releasing/storing oxygen [12–15]. Moreover, CrO_x was used as the most active metals for complete oxidation [16,17]. In addition, we have found that the introduction of Cr into the ceria–zirconia lattice could improve its catalytic activity in our previous work [18].

Some studies have found that improving the specific surface area of the catalyst can improve the catalytic activity [19–21]. Numerous studies focus on the synthesis of $Ce_xZr_{1-x}O_2$ to increase the specific surface area. For example, Zhao et al. [12] prepared $Ce_xZr_{1-x}O_2$ with the citric sol–gel method, obtaining the surface area of 56 $m^2\ g^{-1}$ with Ce/Zr = 2:1. $Ce_xZr_{1-x}O_2$ was also synthesized by co-precipitation method by many researchers, obtaining the highest surface area of 78 $m^2\ g^{-1}$ with Ce/Zr = 4:1 [22,23]. Trovarelli et al. [24,25] synthesized ceria–zirconia solid solution by adding the aqueous solution of the appropriate cationic surfactant, which possessed high surface area of 235 $m^2\ g^{-1}$. And $Ce_xZr_{1-x}O_2$ could also be prepared via the flame method to possess the high surface area, which reached the largest value of 201 $m^2\ g^{-1}$ [26–28]. At the same time, many MOFs materials were applied for CO_2 capture due

* Corresponding author at: Nanjing University of Science and Technology, School of Chemical Engineering, Nanjing 210094, China. Tel.: +86 25 84315517; fax: +86 25 84315517.
E-mail addresses: caiwei_19880105@163.com (W. Cai), zq304@mail.njust.edu.cn (Q. Zhong), zhaowei1021@126.com (W. Zhao), jpu441@yahoo.com (Y. Bu).

http://dx.doi.org/10.1016/j.apcatb.2014.04.022
0926-3373/

to its high surface area. The reason was that MOFs materials contained the rigid ring ligands with carboxyl groups such as benzene carboxylates [29,30]. Hence, taking the above mentioned into consideration, the benzene-muti-carboxylates could also be used as the precipitants to modify the structure of $Ce_xZr_{1-x}O_2$ to obtain the catalysts with high surface area.

In our current work, $Cr/Ce_xZr_{1-x}O_2$ catalysts were prepared with the benzene-muti-carboxylates as the precipitants. The $Cr/Ce_xZr_{1-x}O_2$ with Ce/Zr = 1:4 exhibited the highest NO conversion in our previous study [31]. Hence, four benzene-muti-carboxylates (benzoic acid, terephthalic acid, trimesic acid and cinnamic acid) were adopted as the precipitants to prepare $Cr/Ce_xZr_{1-x}O_2$ in this study. The crystalline structure, grain sizes, surface areas, the information on the surface electronic states and the adsorption capacity of reactant gas were investigated by XRD, HR-TEM, BET surface area analysis, UV–vis DRS, XPS and NO(O_2)-TPD. The excellent catalytic performance which maintained at 60% NO conversion was obtained over this catalyst. The goal was to establish the composition–structure–property relationships, which would provide more insight into design and rationalization of the practical catalysts. Moreover, the reaction mechanism was discussed. In addition, we also investigated the effects of H_2O and SO_2 in flue gases on the activity of the catalysts for NO oxidation.

2. Experimental

2.1. Preparation of the catalysts

All the chemicals were purchased from Alfa Aesar and used as received without further purification. The water used throughout all experiments was purified through a Millipore system. The $Cr/Ce_xZr_{1-x}O_2$ with Ce/Zr = 1:4 was prepared by the co-precipitation method guided by the coordination process. The benzene-muti-carboxylate ligands (benzoic acid, terephthalic acid, trimesic acid and cinnamic acid) were dissolved in deionized water, then NaOH (did not overdose) was added into the solution to form carboxylate radical until pH = 7. The $Ce(NO_3)_3{\cdot}6H_2O$, $ZrOCl_2{\cdot}8H_2O$ and $Cr(NO_3)_3{\cdot}9H_2O$ were mixed in deionized water according to the molar ratio of Ce:Zr:Cr = 2:8:2.56 (Cr was 10% in mass of $Ce_{0.2}Zr_{0.8}O_2$), then the solution was added into the carboxylate radical solution with a 1:1 ratio of the acid to metal ions including Ce^{3+}, Zr^{4+} and Cr^{3+}. The resulting solution was kept in stirring for another 1 h, aged overnight and then centrifuged with distilled water until no pH change. The obtained solids were first dried at 120 °C for 12 h, and then calcined at 500 °C for 6 h to get $Cr–Ce_{0.2}Zr_{0.8}O_2$. For simplification, these catalysts were denoted as CrCZ4-1A, CrCZ4-2A, CrCZ4-3A and CrCZ4-CA, referring to benzoic acid, terephthalic acid, trimesic acid and cinnamic acid as precipitant, respectively. For comparison, the $Ce_{0.2}Zr_{0.8}O_2$ was firstly prepared with cinnamic acid as precipitant according to the above preparation method, then $Ce_{0.2}Zr_{0.8}O_2$ was dispersed in 0.1282 mol L^{-1} (10% in mass) $Cr(NO_3)_3$ aqueous solution. The mixture was kept stirring for 1 h, then refluxed at 60 °C for 4 h. The ovendried product was collected and then calcined at 500 °C for 6 h to obtain the $10Cr/Ce_{0.2}Zr_{0.8}O_2$ catalysts. The obtained catalyst was named as CZ4-CA-Cr.

2.2. Characterizations

The powder XRD patterns were recorded on the Beijing Purkinjie general instrument XD-3 X-ray diffraction using Cu $K\alpha$ radiation at 35 kV and 20 mA (2θ from 5° to 80°). The scanning speed is 8° min^{-1} and the step value is 0.04°.

All IR measurements were performed on a Nicolet-iS10 spectrometer with a resolution of 4 cm^{-1} with 32 co-added scans from 4000 to 400 cm^{-1} in transmission mode at room temperature.

Specific surface areas of the different catalysts were determined by N_2 adsorption–desorption measurements at −196 °C by employing the Brunauer–Emmet–Teller (BET) method (Gold App V-sorb 2008), and the pore volume and pore size of the samples were calculated by Barrett–Joyner–Halenda (BJH) method. The systematic error calculated for BET surface area, pore volume and pore size was given with the accuracy at ±1 $m^2\,g^{-1}$, ±1 $mm^3\,g^{-1}$ and ±0.1 nm, respectively. Prior to N_2 adsorption, the sample was outgassed at 200 °C for 12 h to desorb moisture adsorbed on the surface and inside the porous network.

The micromorphology of the catalysts was examined on a JEOL JEM-2100 transmission electron microscope (TEM), and the sample was deposited on a copper mesh by means of dipcoating. The acceleration voltage is 200 kV.

Diffuse reflectance spectroscopy (DRS) was carried out on a Shimadzu UV-2550 UV–vis spectrophotometer. $BaSO_4$ was the reference sample and the spectra were recorded in the range of 200–800 nm.

X-ray photoelectron spectra (XPS) was performed on a Thermo ESCALAB 250 (USA) apparatus with Al $K\alpha$ X-rays ($h\nu$ = 1486.6 eV) radiation operated at 150 W to investigate the surface atomic concentrations and the oxidation state distribution of the elements in the samples. All binding energies (BE) were referenced to the adventitious C 1s at 284.4 eV. This reference gave BE values with an accuracy at ±0.1 eV. And the atomic surface ratios of the corresponding species were given with the accuracy at ±0.1%. The penetration depth of the XPS probe is 10 nm.

Temperature-programmed desorption (TPD) was carried out on automated chemisorption analyzer (Quantachrome Instruments). About 200 mg of sample was used. After NO (or O_2) saturation in 1 h, the gas was switched to He for 0.5 h. Subsequently, TPD was performed by ramping the temperature at 10 °C min^{-1} to 800 °C in He (70 mL min^{-1}). Desorption of NO (O_2) was detected by a thermal conductivity detector (TCD).

The DRIFTS spectra were acquired using an in situ DRIFTS cell equipped with a gas flow system. DRIFTS measurements were performed with Nicolet iZ10 FTIR spectrometers at 4 cm^{-1} resolution with 32 co-added scans. In the DRIFTS cell, the catalyst was pretreated at 300 °C in He for 2 h and then cooled to the 250 °C. After the background spectrum was recorded with the flowing of He and was subtracted, the sample was exposed to 4000 ppm NO and followed by exposed to 4000 ppm NO + 8% O_2 and the DRIFTS spectra were recorded.

H_2 temperature-programmed reduction (H_2-TPR) was conducted on an American Quantachrome to study the reducibility of the catalysts. TPR measurements were carried out on 100 mg of catalyst, and heated from room temperature to 50 °C for 30 min to pretreatment under N_2 stream (70 mL min^{-1}). Then, the reduction of H_2 was conducted in an H_2–N_2 (10% H_2) mixture (70 mL min^{-1}) for 1 h. Then the sample was heated with a heating rate of 10 °C min^{-1} from 50 °C to 600 °C after datum line was flat. The amount of consumed H_2 was measured by a thermal conductivity detector (TCD).

2.3. Catalytic activity test

The catalytic oxidation of NO was performed in a fixed-bed flow microreactor at atmospheric pressure. Typically, 300 mg sample (sieve fraction of 40–60 mesh) was placed in a quartz reactor (6.8 mm i.d.); the reactant gas mixture (390 ppm NO, 8% O_2, 300 ppm SO_2 (when used), 6 vol.% water (when used), N_2 balance) was fed to the reactor with a total flow rate of 100 mL min^{-1}, corresponding to a gas hour space velocity (GHSV) of 35,400 h^{-1}. The

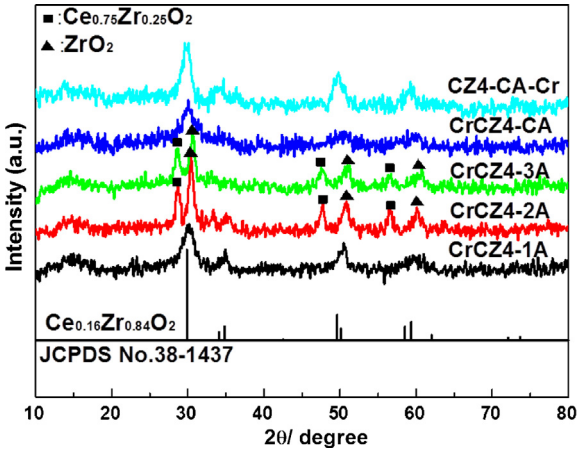

Fig. 1. XRD patterns of CrCZ4-*x*A catalysts with different precipitant and CZ4-CA-Cr catalyst.

steady-state tests were conducted isothermally every 50 °C from 200 °C to 400 °C and the gas products (after 90 min reaction) were analyzed by a Ecom-JZKN flue gas analyzer (Germany). The NO conversion is defined as:

$$\mathrm{NO\,conversion\,to\,NO_2} = (\mathrm{NO_{in}} - \mathrm{NO_{out}})/\mathrm{NO_{in}} \times 100\%$$

And the NO_2 selectivity is defined as:

$$\mathrm{NO_2\,selectivity} = (\mathrm{NO_{2out}} - \mathrm{NO_{2in}})/(\mathrm{NO_{in}} - \mathrm{NO_{out}}) \times 100\%$$

Deserved to be mentioned, the numbers of relevant digits behind the decimal point in the calculated results are selected as 2.

3. Results and discussion

3.1. Structural characterization (XRD, TEM, BET)

3.1.1. XRD analysis

The powder XRD patterns of the catalysts were shown in Fig. 1. CrCZ4-1A, CrCZ4-CA and CZ4-CA-Cr presented the tetragonal structure at 29.9°, 34.7°, 50.1° and 59.4°, corresponding to the (1 1 1), (2 0 0), (2 2 0), and (3 1 1) planes [24], which was supported by the fact that the position of their peaks was the same as that of $Ce_{0.16}Zr_{0.84}O_2$ peaks (JCPDS No. 38-1437). In addition, the low intensity broad band at 34.7° appeared in CrCZ4-CA and CZ4-CA-Cr could be attributed to the tetragonal contributions of the (0 0 2) and (2 0 0) planes. However, CrCZ4-2A and CrCZ4-3A showed the mixed crystallization of $Ce_{0.75}Zr_{0.25}O_2$ and ZrO_2. The phenomenon could be attributed to the long distance between the carboxylate radical of terephthalic acid and trimesic acid while they were used as the precipitants. The distances between the carboxylate radicals of terephthalic acid and trimesic acid were about 7.144 Å and 6.458–6.466 Å, respectively, which were higher than the lattice parameter of $Ce_{0.2}Zr_{0.8}O_2$ (5.18 Å). The distances were measured after the molecule geometries of terephthalic acid and trimesic acid were calculated by the DMol3 module with the generalized gradient approximation (GGA), using the functional PW91 in combination with the double numerical polarized (DNP) basis set. Due to the long distance between the carboxylate radicals of terephthalic acid and trimesic acid, the stronger polarized Zr^{4+} [32] could first interact with the carboxylate radicals and interacted with Ce^{3+} to form $Ce_xZr_{1-x}O_2$ precursor, leading to the mixed crystallization of CrCZ4-2A and CrCZ4-3A. Moreover, comparing to CrCZ4-CA and CZ4-CA-Cr, it could be seen that the diffraction peak was broader over CrCZ4-CA, which indicated that the particle sizes of CrCZ4-CA were smaller. The results demonstrated that the one-pot method (CrCZ4-CA) was not only simple but also beneficial for the generation of small grain size. On the other hand, among the prepared catalysts, no peaks of CrO_x were detected, suggesting a better dispersion of CrO_x crystallites on the $Ce_xZr_{1-x}O_2$ matrix.

3.1.2. TEM analysis

The transmission electron microscopy (TEM) imagines and selected area electron diffraction (SAED) images of all the samples were shown in Fig. 2. It could be seen that all the samples were agglomerated due to the small grain size, and the catalysts prepared with cinnamic acid as precipitant showed the smallest grain size. However, the pore structure formed by the accumulation of small particles increased the surface area. In other studies [33,34], the particles of $Ce_xZr_{1-x}O_2$ were also small but agglomerated, and the particles with the narrowest distributed was around 5.1 ± 0.5 nm, which was similar to the particle size in our work.

In addition, compared CrCZ4-CA with CZ4-CA-Cr, it could be seen that the agglomerate was more serious over CZ4-CA-Cr, which indicated that one-pot method was beneficial for the dispersion of grain sizes. It was obvious that two kinds of particles appeared in CrCZ4-2A and CrCZ4-3A, which supported the XRD results. Moreover, the pore structures formed by the accumulation of small particles disappeared during the formation of large particles. For CrCZ4-1A (Fig. 2(A2)), only one type of periodicity of lattice fringes (~0.295 nm) could be observed, which corresponded to the (1 1 1) plane of $Ce_{0.16}Zr_{0.84}O_2$. The continuous rings in the selected area diffraction (SAED) pattern (Fig. 2(A3)) indicated the presence of the tetragonal phase, as shown in the (2 0 0) facet with the spacing of 0.265 nm [35]. Although there were mixed phases appeared in CrCZ4-2A and CrCZ4-3A, the major patterns of the nanocrystals imaged in the SAED (Fig. 2(B2, B3, C2 and C3)) could again be indexed to the fluorite structure they were also enclosed by the (1 1 1) plane with the interplanar spacing of 0.299–0.309 nm. In addition, the diffraction pattern of CrCZ4-2A and CrCZ4-3A were not continuous, which was due to the appearance of ZrO_2. For CrCZ4-CA and CZ4-CA-Cr (Fig. 2(D2 and E2)), the block-shaped pattern clearly presented the (1 1 1) lattice planes with an interplanar spacing between 0.301 and 0.308 nm. From the SAED patterns (Fig. 2(D3 and E3)), the pseudocubic structure could be identified [19,36]. Notably, the (1 1 1) plane was predominate in all samples.

3.1.3. BET analysis

Some studies have found that improving the texture properties (such as specific surface area) of the catalyst was beneficial for improving the catalytic activity [19–21]. The N_2 adsorption–desorption isotherms of the five prepared catalysts were shown in Fig. 3(a). CrCZ4-1A, CrCZ4-CA and CZ4-CA-Cr showed isotherms of type IV [37], which were similar to isotherms of type I. Moreover, they exhibited hysteresis loops of type H4, indicating that these samples contained mesopores (2–50 nm) and a certain amount of micropores (<2 nm) with narrow cranny-like shapes [38]. Moreover, CrCZ4-2A and CrCZ4-3A showed isotherms of type IV, and they exhibited hysteresis loops of type H3, which indicated that these samples contained mesopores (2–50 nm) with narrow slit-like shapes [38].

The corresponding pore size distributions in the mesoporous region were shown in Fig. 3(b), which were calculated by the BJH method. It could be seen from the pore size distributions that CrCZ4-1A, CrCZ4-CA and CZ4-CA-Cr were consisted of small particle pores (≤4 nm) while CrCZ4-2A and CrCZ4-3A contained large particle pores. Moreover, CrCZ4-CA displayed microporous structure, shown in the inset of Fig. 3(b).

As shown in Table 1, the CrCZ4-1A, CrCZ4-CA and CZ4-CA-Cr showed, respectively, a higher specific surface area than that of CrCZ4-2A and CrCZ4-3A, which can be attributed to the adsorption of reactant gas. The reasons could be suggested as the mentioned

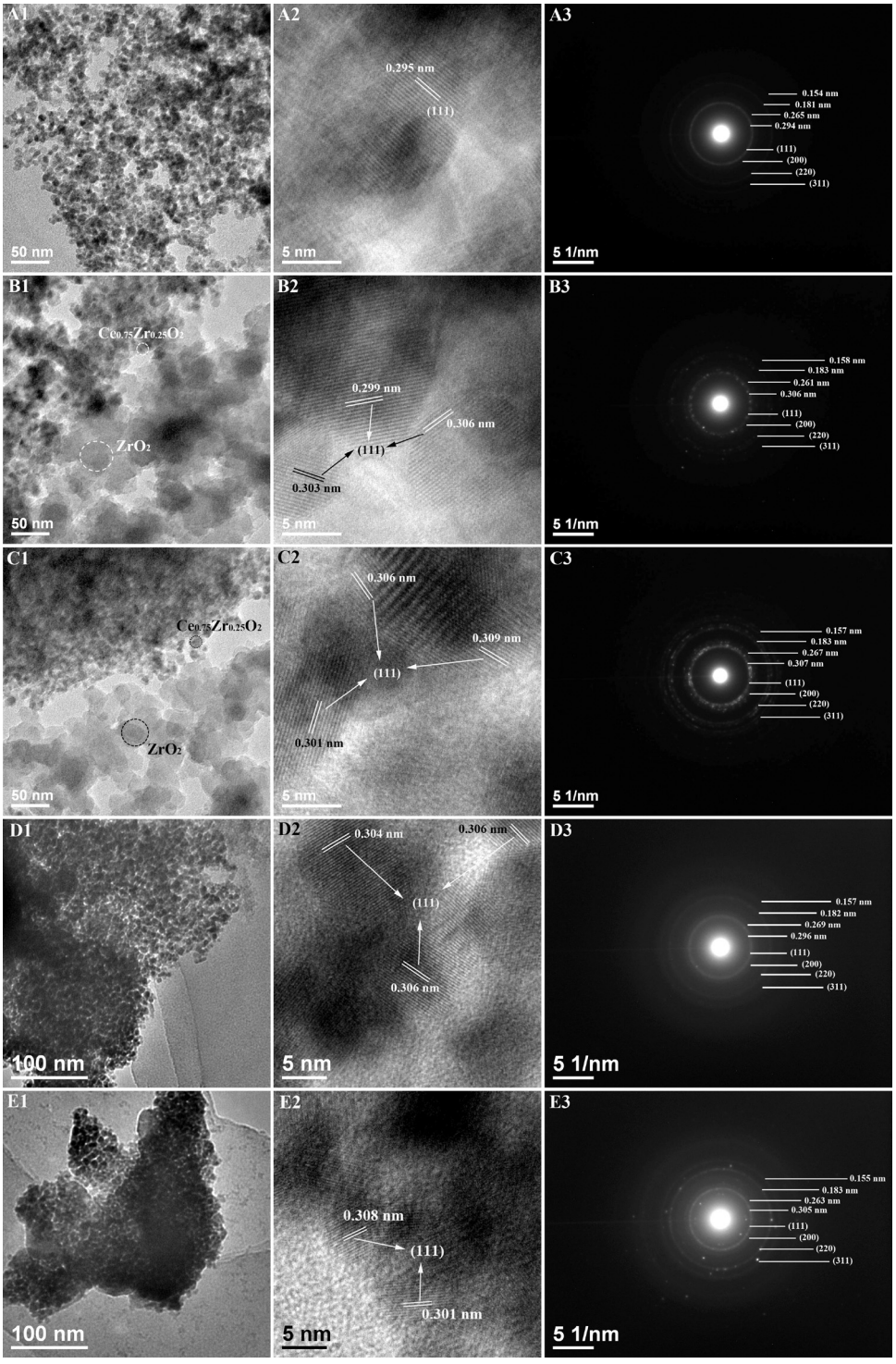

Fig. 2. TEM, HR-TEM and selected area electron diffraction (SAED) images of CrCZ4-*x*A catalysts with different precipitant and CZ4-CA-Cr catalyst. (A) CrCZ4-1A; (B) CrCZ4-2A; (C) CrCZ4-3A; (D) CrCZ4-CA; (E) CZ4-CA-Cr.

Table 1
The surface area and pore structure parameters of CrCZ4-*x*A catalysts with different precipitant and CZ4-CA-Cr catalyst.

	CrCZ4-1A	CrCZ4-2A	CrCZ4-3A	CrCZ4-CA	CZ4-CA-Cr
BET ($m^2\ g^{-1}$)	100	28	59	125	59
Pore volume ($mm^3\ g^{-1}$)	115	90	140	73	72
Pore size (nm)	4.1	9.7	6.4	3.3	4.0

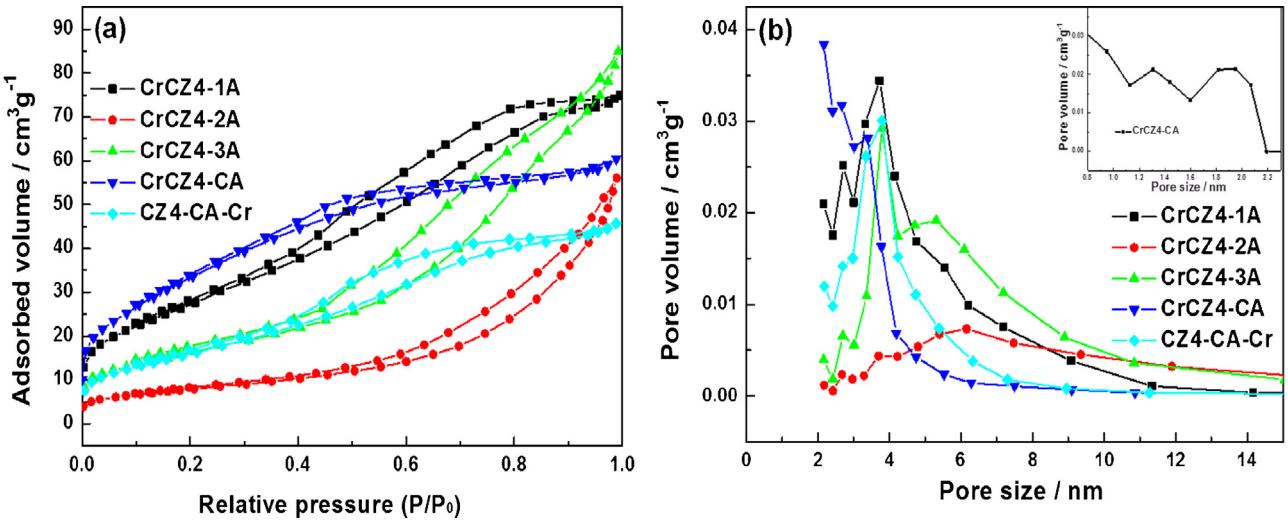

Fig. 3. N_2 adsorption–desorption isotherms (a) and pore size distributions (b) of CrCZ4-*x*A catalysts with different precipitant and CZ4-CA-Cr catalyst. The inset shows the pore size distributions of CrCZ4-CA calculated by HK method in the range 0.8–2.3 nm at high magnification.

below. One-pot method could possess the higher surface area than the impregnation method, which was due to that Cr species were added into the solution, and interacted with the carboxylate radical together with Ce and Zr. Thus Cr species could help to generate the porous structure after calcinations. But in the impregnation method, Cr species occupied the porous structure formed by the calcinations of the precursor $Ce_{0.2}Zr_{0.8}O_2$, thus leading the decrease of surface area. However, CrCZ4-2A and CrCZ4-3A showed the relatively low surface area, which was attributed to the appearance of the mixed crystallization in CrCZ4-2A and CrCZ4-3A (supported by the XRD and TEM results). The particle sizes were heterogeneous in the mixed crystallization, thus leading the decrease of surface area. Moreover, due to the charge balance in the cinnamic acid-contained solution, caused by the π–π conjugated effect of the cinnamic acid, Cr species could interact with the carboxylate radical together with Ce and Zr more uniformly than in the benzoic acid-contained solution. Hence, the surface area of CrCZ4-CA was higher than that of CrCZ4-1A.

The results were in accord with TEM analysis. Moreover, CrCZ4-CA showed the highest surface area and the smallest average pore diameter among the prepared catalysts. Interestingly, the specific surface area of CrCZ4-CA was higher than that of CZ4-CA-Cr. The phenomena could be due to that Cr species were added into the solution, and interacted with the cinnamic acid together with Ce and Zr. Thus Cr species could help to generate the porous structure after calcinations. However, in CZ4-CA-Cr, Cr species occupied the porous structure formed by the calcinations of the precursor $Ce_{0.2}Zr_{0.8}O_2$, thus leading the decrease of surface area.

3.2. Chemical and electronic states of CrCZ4-xA and CZ4-CA-Cr catalysts (UV, XPS)

3.2.1. UV–vis diffuse reflectance measurements analysis

The information on the surface electronic states can be obtained from UV–vis diffuse reflectance measurements. As shown in Fig. 4(a), two bands from CrCZ4-1A, CrCZ4-2A and CrCZ4-3A at ca. 274 and 366 nm could be attributed to $O_2 \rightarrow Ce^{4+}$ charge transfer and interband transitions [39], whereas only a broad one around 366 nm appeared in CrCZ4-CA and CZ4-CA-Cr. The absorption band at ca. 255 nm corresponding to the $O_2 \rightarrow Ce^{3+}$ charge transfer transition [20] was not clearly observed. Eight-coordinated tetravalent Zr species (like those of cubic and tetragonal zirconia) contributed to the absorption in the range 200–220 nm [40], shown in the dash area in Fig. 4(a). However, two other bands appeared in CZ4-CA-Cr. The band at ca. 467 nm could be assigned to Cr^{3+} in Cr_2O_3 [41] and also to the transition $^1T_2 \leftarrow {}^1A_1$ ($^1t_1 \rightarrow 2e$) of a Cr^{6+} species anchored to the support surface as a chromate anion, and/or contained within dichromate species. The band at ca. 588 nm was generally assigned to Cr^{3+} in Cr_2O_3 [41]. Due to Cr species were added into the solution with Ce and Zr at the same time, Cr elements could be doped into the ceria–zirconia solid solution, thus the two bands did not appear in CrCZ4-*x*A. The energy band gaps of these catalysts were shown in the inset of Fig. 4(b). The band gap sizes of CrCZ4-1A, CrCZ4-2A, CrCZ4-3A, CrCZ4-CA and CZ4-CA-Cr were 2.40, 2.69, 2.57, 2.33 and 2.31 eV, respectively. In Liu's study [22], it could be found that the highest position of absorption edges was located in 527 nm over $Ce_{0.5}Zr_{0.5}O_2$. Thus the corresponding lowest band gap was 2.35 eV, which was a little larger than that of the catalysts prepared with cinnamic acid as precipitant. The results indicated that the band gap was influenced by the structure of the prepared catalysts. Due to the mixed crystallization, the band gaps of CrCZ4-2A and CrCZ4-3A were much higher than others. Moreover, the π–π conjugated effect of the cinnamic acid caused the charge balance in the precursor of CrCZ4-CA and CZ4-CA-Cr. Hence, the band gaps of CrCZ4-CA and CZ4-CA-Cr were lower than that of CrCZ4-1A after calcinations. In addition, the band gap of CrCZ4-CA was close to that of CZ4-CA-Cr, which further confirmed the above inference.

3.2.2. XPS analysis

The catalyst systems were analyzed by XPS to verify surface composition and elementary oxidation states. The complex spectrum of Ce 3d was decomposed into eight components with peak assignments in Fig. 5. The chemical valence of cerium on the surface of $Ce_xZr_{1-x}O_2$ was mainly in a +4 oxidation state, and a small quantity of Ce^{3+} (u', v') co-existed [20,42,43]. The enhancement of homogeneity of the Ce and Zr atoms could improve the valence change of the Ce ($Ce^{4+} \rightarrow Ce^{3+}$) [44]. Another reason was probably due to the substitution of Ce^{4+} by Zr^{4+} ions or Cr^{3+} ions partly in the coprecipitation process. The spontaneous transformation of Ce^{4+} ($r_{Ce^{4+}} = 0.97$ Å) ion to the larger Ce^{3+} ($r_{Ce^{3+}} = 1.10$ Å) could compensate for this lattice contraction. The relative intensities of u' and v' to the whole eight bands were 9.7%, 7.5%, 12.6%, 20.4% and 22.9%, referring to CrCZ4-1A, CrCZ4-2A, CrCZ4-3A, CrCZ4-CA and CZ4-CA-Cr, respectively, which was shown in Table 2. Obviously, the surface

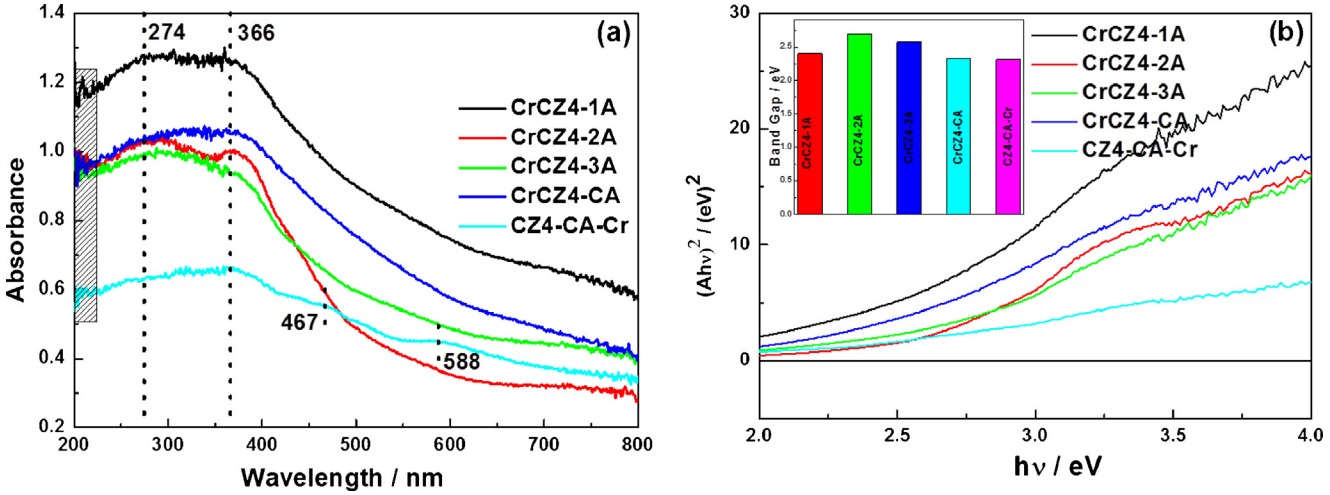

Fig. 4. UV–vis absorption spectra (a) and the energy of band gap (b) of CrCZ4-*x*A catalysts with different precipitant and CZ4-CA-Cr catalyst.

ratios of Ce^{3+} to (Ce^{3+} + Ce^{4+}) on the catalysts prepared with cinnamic acid as precipitant were higher than others, which indicated that there was more incorporation of zirconia on CrCZ4-CA and CZ4-CA-Cr. The charge balance in the precursor of CrCZ4-CA and CZ4-CA-Cr caused by the π–π conjugated effect of the cinnamic acid led to the reduction of peak intensities than that of others after calcinations.

The Zr $3d_{3/2}$ and Zr $3d_{5/2}$ were observed around 184 eV and 181 eV, respectively, over all the catalysts. Interestingly, the binding energy of the latter was higher than that in Zr metal (180.0 eV),

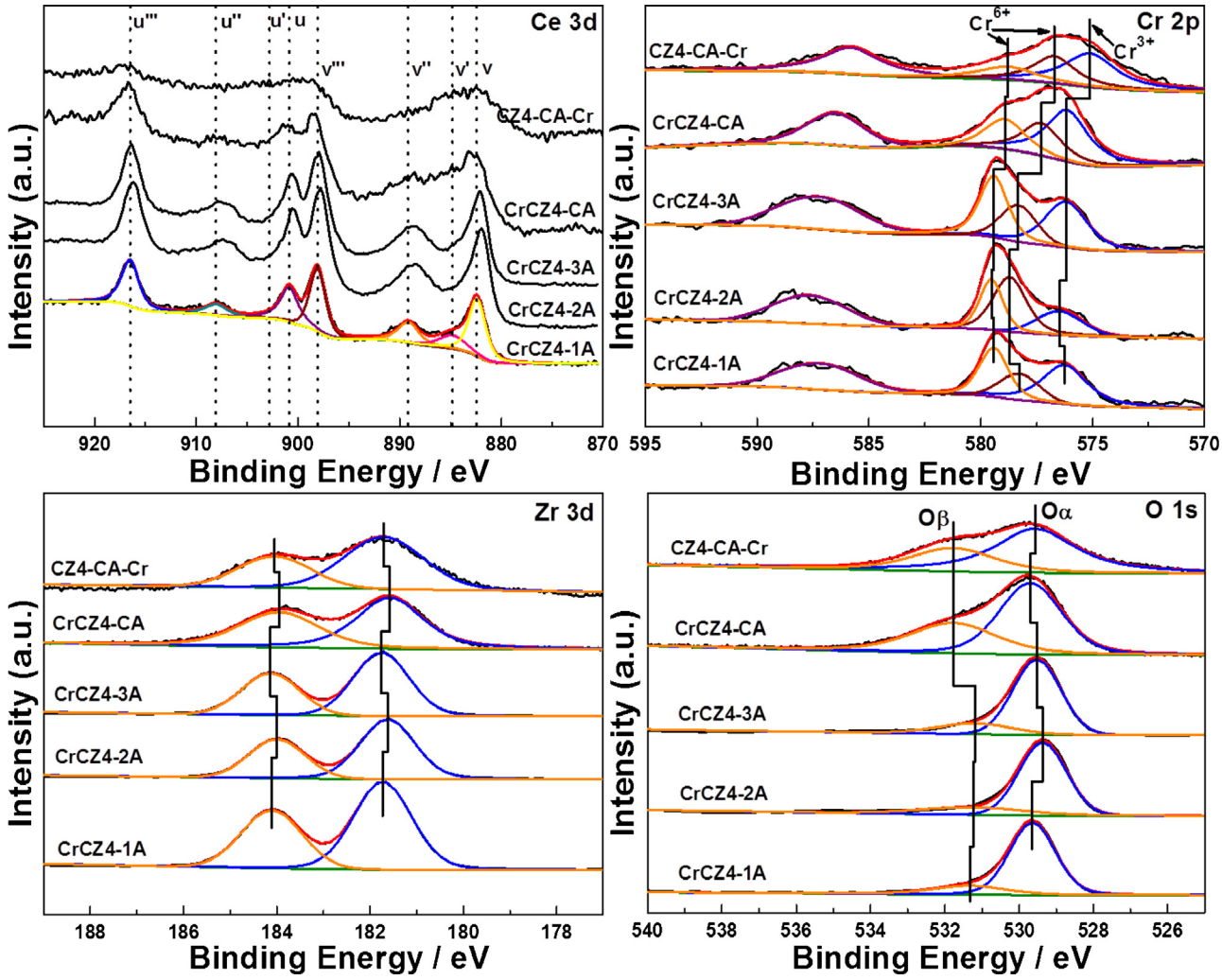

Fig. 5. XPS spectra (Ce 3d, Cr 2p, Zr 3d, O 1s) of CrCZ4-*x*A catalysts with different precipitant and CZ4-CA-Cr catalyst.

Table 2
XPS elementary atomic surface ratios of CrCZ4-*x*A catalysts with different precipitant and CZ4-CA-Cr catalyst.

Samples	Atomic ratios		
	$Ce^{3+}/(Ce^{3+}+Ce^{4+})$ (%)	$Cr^{6+}/(Cr^{6+}+Cr^{3+})$ (%)	$O_\beta/(O_\alpha+O_\beta)$ (%)
CrCZ4-1A	9.7	54.5	19.4
CrCZ4-2A	7.5	56.5	20.5
CrCZ4-3A	12.6	59.9	19.2
CrCZ4-CA	20.4	51.9	39.0
CZ4-CA-Cr	22.9	52.0	37.8

lower than that in ZrO_2 (182.9 eV), but similar to that in ZrO_x ($0<x<2$, 181.4 eV) [40]. Hence, the Zr 3d analysis also proved the displacement of Zr^{4+} ions into the ceria lattice.

From the Cr 2p XPS spectra, it could be seen that two peaks at about 587 and 576 eV that were assigned to $2p_{1/2}$ and $2p_{3/2}$ of Cr^{3+} species, respectively [45]. The peaks at about 579 and 578 eV were assigned to $2p_{3/2}$ of Cr^{6+} species. The former was in the form of $Cr_2O_7^{2-}$ species, the latter was from CrO_3 species. It was obvious that all the binding energies of the catalysts prepared with cinnamic acid as precipitant were lower than other catalysts. It was due to the charge balance in the precursor of CrCZ4-CA and CZ4-CA-Cr caused by the π–π conjugated effect of the cinnamic acid, which was in accord with the analysis of Ce 3d. Hence, the relative intensities of Cr^{6+} in CrCZ4-CA and CZ4-CA-Cr were lower than others, which were shown in Table 2.

O 1s spectra were mainly composed of two components. The high-resolution spectrum for the O 1s ionization features was numerically fitted with the Gaussian features representing the primary O 1s ionization feature and chemically shifted O 1s features from chemisorbed surface species such as O_2^- and O^-. The strong band O_α (around 529 eV) was attributed to the characteristic oxygen peak of the metal oxides [46], while the shoulder O_β with higher binding energy (around 531 eV) was the result of chemisorbed oxygen [47]. Obviously, the ratios of chemisorbed oxygen to the whole type of oxygen in CrCZ4-CA and CZ4-CA-Cr exhibited the highest (Table 2), which indicated that the cinnamic acid as precipitant in preparation was beneficial for the formation of oxygen vacancy in the oxide surface.

3.3. Adsorption properties (NO-TPD, O_2-TPD)

TPD experiments were conducted to test the reversibility of NO (or O_2) adsorption. The TPD profiles of NO on the CrCZ4-*x*A catalysts with different precipitants and CZ4-CA-Cr were shown in Fig. 6(a). As the temperature increased from 50 to 600 °C, NO gas desorption was observed on these catalysts. All of these samples showed two main temperature ranges (α and β) for NO desorption, suggesting that NO adsorbed on two different sites [48]. α desorption peak located at ~150 °C was assigned to monodentate nitrate and bridged nitrate, and β desorption peak located at ~380 °C was assigned to bridged nitrate and bidentate nitrate [49]. Moreover, the NO desorption ability was consistent with NO capacities of these sorbents, i.e., CrCZ4-CA > CZ4-CA-Cr > CrCZ4-1A > CrCZ4-3A > CrCZ4-2A. The results indicated that the abilities of surface adsorption desorption NO over catalysts prepared with cinnamic acid as precipitant were stronger than that of other catalysts. The reasons might be due to the mixed phase of CrCZ4-2A and CrCZ4-3A caused by the long distances between the carboxylate radical of terephthalic acid and trimesic acid. In addition, the adsorbed NO was easy to be desorbed in the temperature range from 100 °C to 200 °C, which indicated that the adsorption NO was weak.

Generally, there were three kinds of active oxygen species: γ, δ and ε on surface of $Ce_xZr_{1-x}O_2$. γ O species had a lower desorption temperature (<350 °C), which can be assigned to the chemical adsorption oxygen; ε O species had a higher desorption temperature (>750 °C), being assigned to the oxygen in the crystal lattice. However, the desorption temperature of δ O species was between these two desorption temperatures, which was related with oxygen defect and was considered as partial crystal oxygen [50].

The O_2-TPD profiles were shown in Fig. 6(b). For all catalysts, the desorption profiles of O_2 were observed over the wide temperature range from 80 to 800 °C. Obviously, all catalysts showed two desorption peaks of γ and δ, and CrCZ4-CA and CrCZ4-1A showed the desorption peak of ε. However, compared the five catalysts, CrCZ4-CA showed the highest adsorption capacity of δ O species, and CZ4-CA-Cr showed the highest adsorption capacity of γ O species. The results indicated that the catalyst prepared with cinnamic acid as precipitant had more chemical adsorption oxygen and oxygen defect on its surface.

3.4. NO oxidation activity

The catalytic activities and NO_2 selectivity of CrCZ4-*x*A catalysts with different precipitants and CZ4-CA-Cr catalyst were shown in

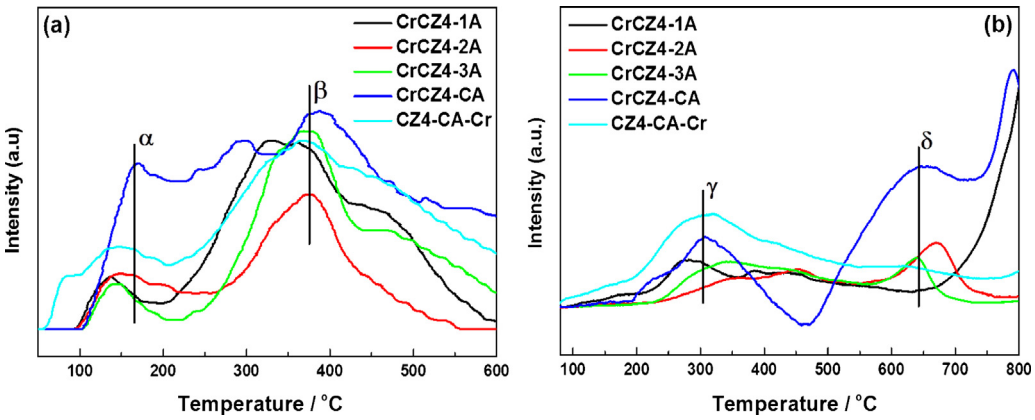

Fig. 6. NO-TPD (a) and O_2-TPD (b) of CrCZ4-*x*A catalysts with different precipitant and CZ4-CA-Cr catalyst.

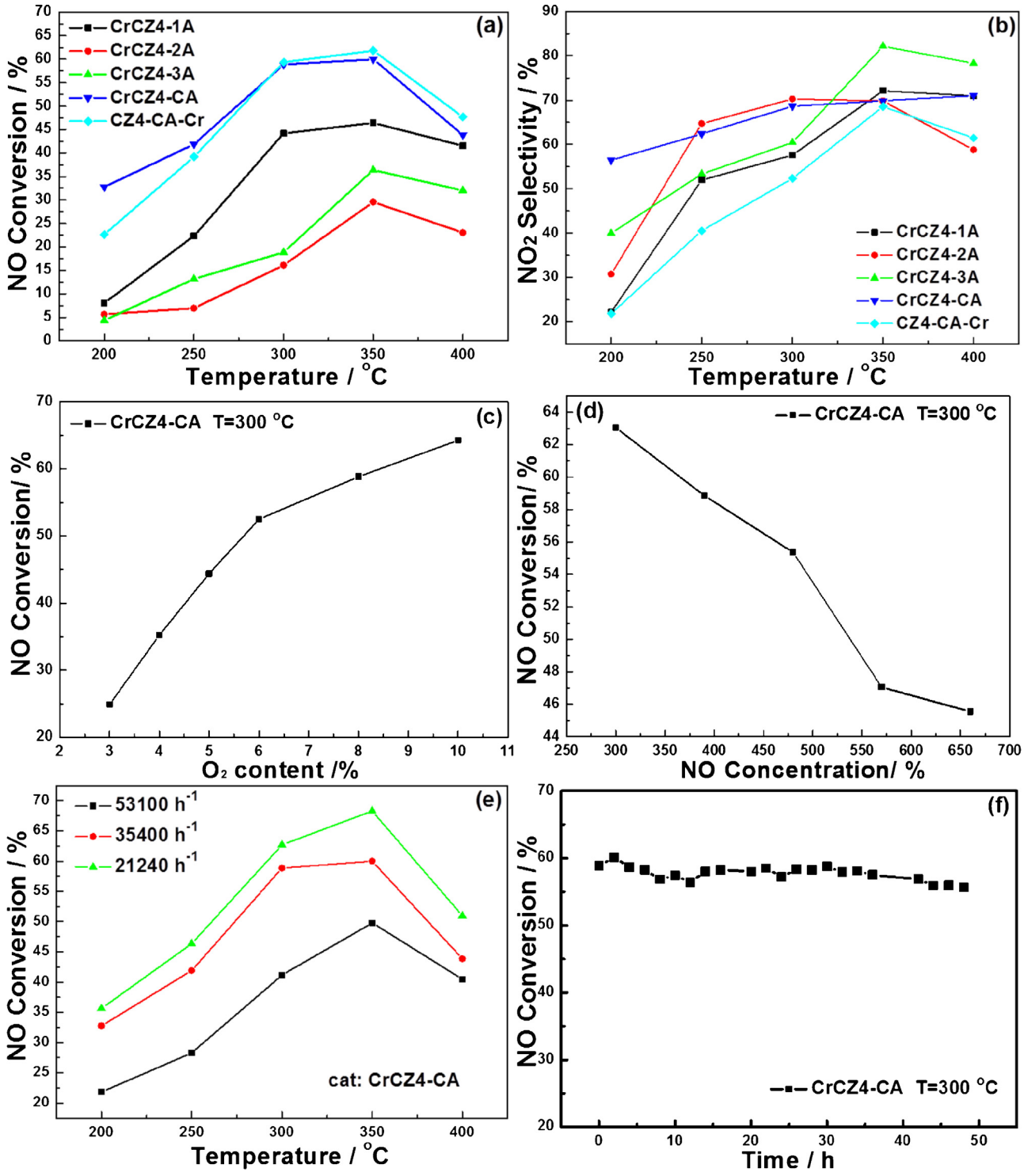

Fig. 7. (a and b) Catalytic performance and NO_2 selectivity of CrCZ4-*x*A catalysts with different precipitant and CZ4-CA-Cr catalyst. Reaction conditions: 390 ppm NO, 8% O_2, N_2 as balance gas, GHSV = 35,400 h^{-1}; (c and d) the effect of O_2 and NO concentration on NO conversion over CrCZ4-CA. Reaction conditions: N_2 as balance gas, GHSV = 35,400 h^{-1}, T = 300 °C; (e) the catalytic activity of CrCZ4-CA in a range of GHSV from 21,240 to 53,100 h^{-1}. Reaction conditions: 390 ppm NO, 8% O_2, N_2 as balance gas; (f) the stability test over CrCZ4-CA at 300 °C for 48 h. Reaction conditions: 390 ppm NO, 8% O_2, N_2 as balance gas, GHSV = 35,400 h^{-1}.

Fig. 7(a and b). It was obvious from Fig. 7(a) that all catalysts showed the best catalytic activity at 350 °C. Moreover, the catalysts prepared with cinnamic acid as precipitant exhibited the highest NO conversion, and the best oxidation efficiency ranges were broader than that of others, especially than that of CrCZ4-2A and CrCZ4-3A. Moreover, it could be found that NO conversion over CZ4-CA-Cr was slightly better than that over CrCZ4-CA, which reached 61.84% at 350 °C. The conversion reached the best oxidation efficiency in the report [9,11]. However, the preparation process of CrCZ4-CA was simpler. The conversion decreased slowly as the result of the decomposition of NO_2 at 350–400 °C. In some previous study, NO conversion reached only about 30% at 450 °C in the condition of GHSV = 30,000 h^{-1} over $Ce_xZr_{1-x}O_2$ [51]. In other studies, NO conversion reached about 60% at 150 °C over Mn–Ce–O_x catalysts [52], and reached about 90% at 300 °C over Pt/TiO_2 [53]. Due to the low SO_2 resistance over Mn-based catalysts and the high cost for

preparation over Pt-based catalysts, these catalysts could not be applied for the NO_x removal in the coal power plant, but they could be applied for other NO_x removal, such as automobile exhaust treatment and diesel oxidation.

Notably, the oxidation efficiencies of CrCZ4-CA and CZ4-CA-Cr were much higher than other catalysts. However, the NO_2 selectivity over these catalysts was similar (shown in Fig. 7(b)), and most of them exhibited the highest NO_2 selectivity at 350 °C except for CrCZ4-CA. The NO_2 selectivity over CrCZ4-CA increased slightly with the increasing of temperature, and it kept at about 60% from 200 to 400 °C.

It was known from previous studies that O_2 had significant effect on NO oxidation [54]. Hence, the effect of O_2 concentration on NO conversion of CrCZ4-CA has been studied as shown in Fig. 7(c). In the low O_2 concentration range, the NO conversion increased sharply from 24.92% to 52.5% while the O_2 concentration was from 3% to 6%. The NO conversion almost maintained the same as the O_2 concentration in the range of 6% to 10%. The reason of this result was that O_2 improved the NO adsorption over CrCZ4-CA so that the NO concentration in the outlet of fixed-bed flow reactor decreased. The influence of NO concentration on NO conversion of CrCZ4-CA was shown in Fig. 7(d). The oxidation efficiency decreased dramatically while NO concentration increased from 300 ppm to 570 ppm. However, the conversion almost stayed a constant while the NO concentration increased from 570 ppm to 660 ppm. This is due to that the adsorption of NO reached saturation while the NO concentration was too high to reduce the remained active site on the surface of the catalyst, thus leading to reduce the adsorbed amount of O_2. Moreover, the driving force of the reaction increased with the increase of NO concentration, while the amount of NO to be resolved also increased. All these factors contributed to this phenomenon.

The space velocity is crucial for practical applications. Fig. 7(e) displayed the catalytic activity of CrCZ4-CA in a range of GHSV from 21,240 to 53,100 h^{-1}. As shown in Fig. 7(e), the NO conversion increased clearly as GHSV decreased. However, the oxidation efficiency increased slightly while the GHSV decreases from 35,400 to 21,240 h^{-1}. When the GHSV reached 21,240 h^{-1}, CrCZ4-CA exhibited an excellent NO conversion that was 68.29% at 350 °C. The stability test over CrCZ4-CA was conducted for 48 h at 300 °C, which was shown in Fig. 7(f). It was obvious that the NO conversion kept at about 60% with the increasing of time, which indicated that the catalyst could hold the high activity in the long-time reaction process.

3.5. In-situ DRIFTS

Fig. 8 showed the spectra after the introduction of 4000 ppm NO at 250 °C and followed 8% O_2 was introduced. The surface of tested catalysts was covered by two kinds of nitrates: monodentate nitrate (1261 cm^{-1}) and bidentate nitrate (1550 cm^{-1}) [55–57]. In addition, the weak bands at 1845 and 1762 cm^{-1} were also presented, which could be assigned to the weak NO adsorption in the form of NO^+ [10,58]. All the bands described above grew with time, and the intensities reached the strongest after the NO feeding for 30 min. These implied that the formed nitrates and the adsorbed NO were limited over CrCZ4-CA. While O_2 supply was switched on, some new bands formed, including the bands at 3730 and 1380 cm^{-1}. The band at 3730 cm^{-1} was terminated as II-B-Zr and was assigned to —OH connected to two zirconium cations incorporated with the superoxide radical (O_2^-) [59]. The band at 1380 cm^{-1} was in accordance with the literature [60] and assigned to the adsorbed NO_3^-, which was produced by the interaction between chemisorbed NO and the formed O_2^-. However, the intensities of the original formed bands at 1845, 1762, 1550 and 1261 cm^{-1} decreased rapidly with purging 8% O_2, and disappeared after the addition of O_2 for 60 min.

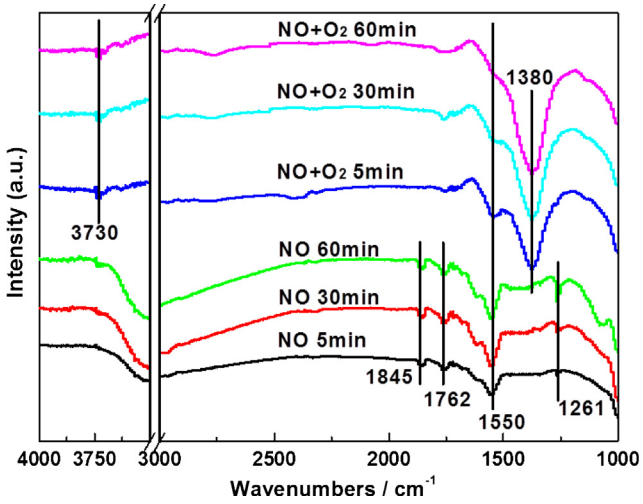

Fig. 8. DRIFTS spectra of CrCZ4-CA under exposure to 4000 ppm NO at 250 °C for various time and followed by exposure to 4000 ppm NO + 8% O_2 for various time.

The results indicated that the formed nitrates and NO^+ had been transferred to other species while O_2 was introduced. Hence, combined to the XPS and TPD analysis, the adsorbed NO interacted with the adsorbed O_2 to generate NO_2 over $Cr/Ce_xZr_{1-x}O_2$, and the reaction mechanism could be shown as below.

$$Cr^{6+} + 3\,NO \rightarrow Cr^{3+} + 3\,NO^+ \quad (1)$$

$$Ce^{3+} \rightarrow Ce^{4+} + e^- \quad (2)$$

$$O_2 + e^- \rightarrow O_2^- \quad (3)$$

$$NO + O_2^- \rightarrow NO_3^- \quad (4)$$

$$NO^+ + NO_3^- \rightarrow 2\,NO_2 \quad (5)$$

$$3\,Ce^{4+} + Cr^{3+} \rightarrow 3\,Ce^{3+} + Cr^{6+} \quad (6)$$

As shown in the above Eqs. (1)–(6), the most probable process of NO oxidation over the $Cr/Ce_xZr_{1-x}O_2$ catalyst could be described as follows: NO was first adsorbed on Cr sites, and then oxidized to NO^+ readily, Eq. (1). At the same time, O_2 was adsorbed on Ce sites, and then it was activated in the process of Ce^{3+} to Ce^{4+} to interact with the released electron to generate oxygen vacancy. The oxygen vacancy interacted with the adsorbed O_2 to form superoxide radical O_2^-, Eqs. (2) and (3). As part of NO was adsorbed into NO^+, the ion pair $NO^+NO_3^-$ could decompose to two NO_2 molecules, Eq. (5) [61]. Finally, the Cr^{3+} was oxidized to Cr^{6+} again by Ce^{4+} at high temperature, Eq. (6).

Moreover, according to the analysis of XPS, it could be found that the content of Cr^{6+} in the samples prepared with cinnamic acid as precipitant were not the highest, but the ratio of Ce^{3+} and O" was higher than others. And the NO conversion over CrCZ4-CA and CZ4-CA-Cr was relatively higher. Hence, it could be concluded that the adsorption and activation O_2 was the key step. This also can be confirmed by the DRIFTS.

In order to confirm the above reaction mechanism further, H_2-TPR and the XPS spectra of the fresh and used CrCZ4-CA were shown in Fig. S1. Two hydrogen consumption peaks (peaks ε and Φ) were detected on the fresh and used catalysts, and the peak positions and the peak areas were nearly the same. According to the literature reported [62,63], the intense peak ε at about 400 °C was ascribed to the reduction of Cr^{6+} to Cr^{5+} or Cr^{3+}, and the peak Φ at about 500 °C was due to the reduction of Ce^{4+} to Ce^{3+}. The results indicated that the corresponding cations remained the same after the test. Moreover, in the figure of H_2-TPR, we could find that the amount of Ce^{4+} decreased a little after the test, which could be deduced that

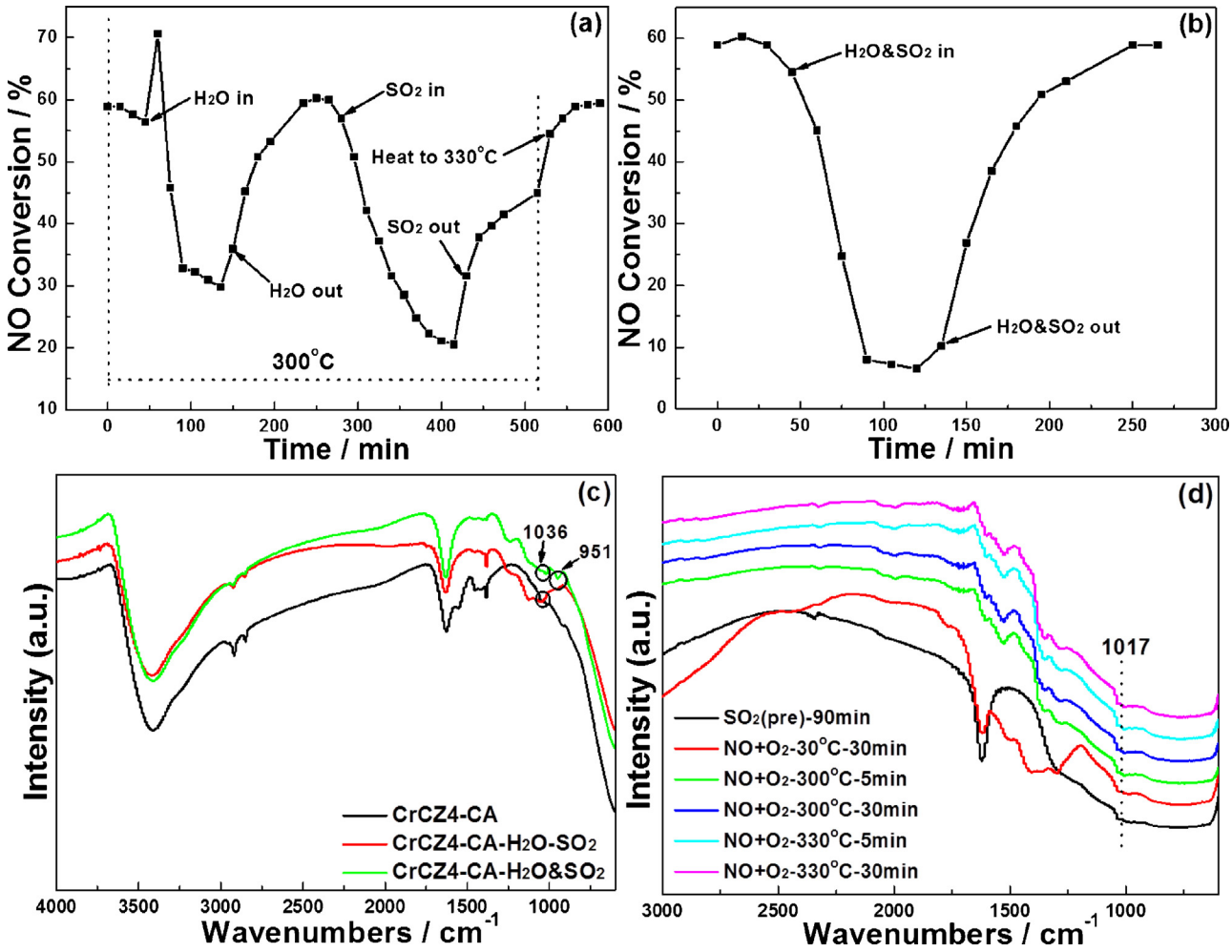

Fig. 9. (a and b) Effect of H_2O and SO_2 on the NO conversion over CrCZ4-CA at 300 °C. Reaction conditions: 390 ppm NO, 8% O_2, 300 ppm SO_2, 6 vol.% H_2O, N_2 as balance gas, GHSV = 35,400 h^{-1}; (c) FT-IR of CrCZ4-CA and H_2O and SO_2-tested CrCZ4-CA; (d) in-situ FT-IR of SO_2-pretreated CrCZ4-CA under exposure to 4000 ppm NO + 8% O_2 at three different temperatures for various time.

Ce^{4+} have been participated the reaction in the test. The results from the curves of XPS could also confirm the above suggestions. In the figure of XPS, the peak positions and the peak areas of the fresh and used catalysts were also nearly the same. And the atomic surface ratios obtained from XPS were shown in Table S1. From Table S1, we can get that the ratios of Ce^{3+}, Cr^{6+} and O_β in the fresh and used catalysts were similar, and the corresponding ratios in the used-CrCZ4-CA were a little higher than that in the fresh catalyst. The results confirm that Ce^{4+} have been participated the reaction to interact with Cr^{3+} to generate Cr^{6+} in the test, which was same to the analysis of H_2-TPR. Thus the reaction mechanism could be described as the above Eqs. (1)–(6).

3.6. Effect of H_2O and SO_2

Effects of H_2O and SO_2 on NO oxidation activities of catalysts investigated as H_2O and SO_2 were the main components in exhaust gas. The impacts of H_2O and SO_2 on NO oxidation over the CrCZ4-CA catalysts were studied, as shown in Fig. 9(a and b). Fig. 9(a) appeared the addition of H_2O to the flue gas can decrease the activity of NO oxidation over CrCZ4-CA. However, the inhibition effect of H_2O on the NO oxidation activity over the catalyst was reversible, while the activity did not recover to the original level in a short time. From the phenomenon, it could be concluded that CrCZ4-CA exhibited the hygroscopicity ability, thus needing a long time period to regain the primary activity. NO oxidation over CrCZ4-CA decreased from 59.97% to 50.79% while SO_2 was added, and the steady state NO conversion was about 20%. Nevertheless, the inhibition effect of SO_2 over CrCZ4-CA was also reversible, while the activity recovery process needed additional heat to 330 °C. Addition of H_2O and SO_2 together suppressed NO oxidation activity to a great extent. Oxidation efficiency decreased from 60% to 8% in the presence of H_2O and SO_2 together. Similar to the above mentioned phenomenon, the inhibition effect of H_2O and SO_2 was reversible as well while H_2O and SO_2 were cut off. Tang et al. [64] studied the effect of SO_2 on NO oxidation over MnO_x/TiO_2 catalyst. The results showed that the catalytic performance decreased while SO_2 was added, and it could not regain the original level while SO_2 was cut off. The reasons could be due to that SO_2 would permanently occupy the active Mn sites as sulfates. In contrast, the $Ce_xZr_{1-x}O_2$-based catalysts prepared in our work showed well SO_2 and H_2O resistance, which was similar to $Ce_xZr_{1-x}O_2$-based catalysts synthesized in other studies [65,66].

To further investigate the poison effect of SO_2 over CrCZ4-CA, H_2O and SO_2-tested catalyst was studied by FT-IR, and SO_2-pretreated catalyst was also studied by in-situ FT-IR under exposure to 4000 ppm NO and 8% O_2, as shown in Fig. 9(c and d). Free SO_4^{2-} ion shows two infrared-active bands at 1104 and 613 cm^{-1} [67], and the inorganic sulfate shows a strong absorption band in the range of 1080–1140 cm^{-1} and a weak but sharp absorption band in the range of 960–1030 cm^{-1} [68]. It could be found from Fig. 9(c

and d) that whether H_2O and SO_2-tested catalyst or SO_2-pretreated catalyst appeared the absorption band at 1036 or 1017 cm^{-1}, which were due to the band of SO_4^{2-} ion. The results indicated that the sulfate existed on the surface of catalyst all the time while SO_2 was added. The competitive adsorption between SO_2 and NO led to the decrease in NO oxidation, but the large surface area was still enough to adsorb NO in the presence of some activity sites occupied by sulfate after SO_2 was cut off [69]. Moreover, due to the adsorption and activation O_2 was the key factor in NO oxidation, oxidation efficiency could be recovered.

4. Conclusion

In summary, the modified $Cr/Ce_{0.2}Zr_{0.8}O_2$ with the rigid benzene-muti-carboxylate ligands was prepared via a simple method for NO oxidation. Combined with XRD, TEM, BET surface area analysis, UV–vis DRS and TPD results, it was demonstrated that the catalysts prepared with cinnamic acid as precipitant showed higher surface area, lower band gap and stronger adsorption capacity of reactant gas, which was due to the charge balance in the precursor of CrCZ4-CA and CZ4-CA-Cr caused by the π–π conjugated effect of the cinnamic acid. And the particle sizes of these catalysts were small but with agglomeration. Moreover, CrCZ4-CA which was synthesized with one-pot method showed the highest surface area, thus leading the high NO conversion and the well ability to resist the poison effect of H_2O and SO_2 over the catalyst. In-situ FTIR results suggested that the adsorbed NO interacted with the adsorbed O_2 to generate NO_2 over $Cr/Ce_{0.2}Zr_{0.8}O_2$, and the adsorption and activation O_2 was the key factor as confirmed by the XPS analysis.

Acknowledgments

This work was financially supported by the National Natural Science Foundation of China (U1162119), the research fund of Key Laboratory for Advanced Technology in Environmental Protection of Jiangsu Province (AE201001), Industry-Academia Cooperation Innovation Fund Projects of Jiangsu Province (BY2012025) and Scientific Research Project of Environmental Protection Department of Jiangsu Province (201112).

Appendix A. Supplementary data

Supplementary data associated with this article can be found, in the online version, at http://dx.doi.org/10.1016/j.apcatb.2014.04.022.

References

[1] Z.Y. Sheng, Y.F. Hu, J.M. Xue, X.M. Wang, J. Rare Earths 30 (2012) 676–682.
[2] C.M.L. Scholz, V.R. Gangwal, M.H.J.M. de Croon, J.C. Schouten, Appl. Catal., B: Environ. 71 (2007) 143–150.
[3] N. Takahashi, K. Yamazaki, H. Sobukawa, H. Shinjoh, Appl. Catal., B: Environ. 70 (2007) 198–204.
[4] Z.Q. Liu, W.S. Epling, J.A. Anderson, J. Phys. Chem. C 115 (2011) 952–960.
[5] Z.H. Liu, Y.S. Ge, J.W. Tan, C. He, J. Environ. Sci. 24 (2012) 624–631.
[6] S.L. Zhang, H.Y. Li, Q. Zhong, Appl. Catal., A: Gen. 435–436 (2012) 156–162.
[7] S.L. Zhang, X.X. Liu, Q. Zhong, Y. Yao, Catal. Commun. 25 (2012) 7–11.
[8] Q. Zhong, T.J. Zhang, Y.T. Li, W.H. Ma, H.X. Qu, Chem. Eng. J. 174 (2011) 390–395.
[9] Z.H. Chen, F.R. Wang, H. Li, Q. Yang, L.F. Wang, X.H. Li, Ind. Eng. Chem. Res. 51 (2012) 202–212.
[10] Y.L. Wang, C.Z. Ge, L. Zhan, C. Li, W.M. Qiao, L.C. Ling, Ind. Eng. Chem. Res. 51 (2012) 11667–11673.
[11] K. Li, X.L. Tang, H.H. Yi, P. Ning, D.J. Kang, C. Wang, Chem. Eng. J. 192 (2012) 99–104.
[12] M.W. Zhao, M.Q. Shen, J. Wang, J. Catal. 248 (2007) 258–267.
[13] I. Atribak, B. Azambre, A. Bueno López, A. García-García, Appl. Catal., B: Environ. 92 (2009) 126–137.
[14] B. Caglar, D. Uner, Catal. Commun. 12 (2011) 450–453.
[15] S.Y. Christou, M.C. Álvarez-Galván, J.L.G. Fierro, A.M. Efstathiou, Appl. Catal., B: Environ. 106 (2011) 103–113.
[16] C.M. Pradier, F. Rodrigues, P. Marcus, M.V. Landau, M.L. Kaliya, A. Gutman, M. Herskowitz, Appl. Catal., B: Environ. 27 (2000) 73–85.
[17] V.N. Panchenko, V.A. Zakharov, E.A. Paukshtis, Appl. Catal., A: Gen. 313 (2006) 130–136.
[18] W. Cai, Q. Zhong, S.L. Zhang, J.X. Zhang, RSC Adv. 3 (2013) 7009–7015.
[19] R.O. Fuentes, R.T. Baker, J. Phys. Chem. C 113 (2009) 914–924.
[20] R. Si, Y.W. Zhang, S.J. Li, B.X. Lin, C.H. Yan, J. Phys. Chem. B 108 (2004) 12481–12488.
[21] C.S. Wright, R.I. Walton, D. Thompsett, J. Fisher, S.E. Ashbrook, Adv. Mater. 19 (2007) 4500–4504.
[22] L.J. Liu, Z.J. Yao, B. Liu, L. Dong, J. Catal. 275 (2010) 45–60.
[23] N. Wang, W. Chu, L.Q. Huang, T. Zhang, J. Nat. Gas Chem. 19 (2010) 117–122.
[24] D. Terribile, A. Trovarelli, J. Llorca, C. Leitenburg, G. Dolcetti, Catal. Today 43 (1998) 79–88.
[25] A. Pappacena, K. Schermanz, A. Sagar, E. Aneggi, A. Trovarelli, Stud. Surf. Sci. Catal. 175 (2010) 835–838.
[26] W.J. Stark, M. Maciejewski, L. Mädler, S.E. Pratsinis, A. Baiker, J. Catal. 220 (2003) 35–43.
[27] R. Strobel, F. Krumeich, S.E. Pratsinis, A. Baiker, J. Catal. 243 (2006) 229–238.
[28] S. Hannemann, J.D. Grunwaldt, P. Lienemann, D. Günther, F. Krumeich, S.E. Pratsinis, A. Baiker, Appl. Catal., A: Gen. 316 (2007) 226–239.
[29] N. Kobayashi, M. Kijima, J. Mater. Chem. 18 (2008) 1037–1045.
[30] M.P. Suh, H.J. Choi, S.M. So, B.M. Kim, Inorg. Chem. 42 (2003) 676–678.
[31] W. Cai, Q. Zhong, S.L. Zhang, W. Zhao, Chem. Eng. J. 236 (2014) 223–232.
[32] W. Cai, Q. Zhong, Y.X. Zhao, Catal. Commun. 39 (2013) 30–34.
[33] S.J. Feng, D. Pan, Z.H. Wang, Adv. Powder Technol. 22 (2011) 678–681.
[34] A. Martínez-Arias, M. Fernández-García, V. Ballesteros, L.N. Salamanca, J.C. Conesa, C. Otero, J. Soria, Langmuir 15 (1999) 4796–4802.
[35] B.M. Reddy, P. Lakshmanan, A. Khan, J. Phys. Chem. B 109 (2005) 13545–13552.
[36] M.P. Yeste, J.C. Hernández, S. Trasobares, S. Bernal, G. Blanco, J.J. Calvino, J.A. Pérez-Omil, J.M. Pintado, Chem. Mater. 20 (2008) 5107–5113.
[37] S. Brunauer, L.S. Deming, W.E. Deming, E. Teller, J. Am. Chem. Soc. 62 (1940) 1723–1732.
[38] K.S.W. Sing, D.H. Everett, R.A.W. Haul, L. Moscou, R.A. Pierotti, J. Rouquérol, T. Siemieniewska, Pure Appl. Chem. 57 (1985) 603–619.
[39] B.M. Reddy, P. Bharali, P. Saikia, J. Phys. Chem. C 112 (2008) 11729–11737.
[40] G. Postole, B. Chowdhury, B. Karmakar, K. Pinki, J. Banerji, A. Auroux, J. Catal. 269 (2010) 110–121.
[41] C.P. Poole, J.F. Itzel, J. Chem. Phys. 39 (1963) 3445–3455.
[42] M. Alifanti, B. Baps, N. Blangenois, J. Naud, P. Grange, B. Delmon, Chem. Mater. 15 (2003) 395–403.
[43] A.E. Nelson, K.H. Schulz, Appl. Surf. Sci. 210 (2003) 206–221.
[44] Y. Nagai, T. Yamamoto, T. Tanaka, S. Yoshida, T. Nonakaa, T. Okamotoa, A. Suda, M. Sugiura, Catal. Today 74 (2002) 225–234.
[45] R. Dholam, N. Patel, A. Santini, A. Miotello, Int. J. Hydrogen Energy 35 (2010) 9581–9590.
[46] G. Avgouropoulos, T. Ioannides, Appl. Catal., B: Environ. 67 (2006) 1–11.
[47] B.M. Reddy, K.N. Rao, P. Bharali, Ind. Eng. Chem. Res. 48 (2009) 8478–8486.
[48] H.Y. Huang, R.T. Yang, Langmuir 17 (2001) 4997–5003.
[49] L.J. Liu, B. Liu, L.H. Dong, J. Zhu, H.Q. Wan, K.Q. Sun, B. Zhao, H.Y. Zhu, Lin Dong, Y. Chen, Appl. Catal., B: Environ. 90 (2009) 578–586.
[50] Z. Zhao, X.G. Yang, Y. Wu, Appl. Catal., B: Environ. 8 (1996) 281–297.
[51] I. Atribak, N. Guillén-Hurtado, A. Bueno-López, A. García-García, Appl. Surf. Sci. 256 (2010) 7706–7712.
[52] H. Li, X.L. Tang, H.H. Yi, L.L. Yu, J. Rare Earths 28 (2010) 64–68.
[53] L.D. Li, Q. Shen, J. Cheng, Z.P. Hao, Appl. Catal., B: Environ. 93 (2010) 259–266.
[54] J. Zhang, H. Li, Z. Tong, Nat. Sci. J. Xiangtan Univ. 33 (2011) 65–72.
[55] F. Liu, H. He, J. Phys. Chem. C 114 (2010) 16929–16936.
[56] L.Q. Nguyen, C. Salim, H. Hinode, Appl. Catal., B: Environ. 96 (2010) 299–306.
[57] G. Jing, J. Li, D. Yang, J. Hao, Appl. Catal., B: Environ. 91 (2009) 123–134.
[58] P. Pietrzyk, K. Podolska, Z. Sojka, J. Phys. Chem. C 115 (2011) 13008–13015.
[59] J. Ouyang, H.M. Yang, J. Phys. Chem. C 113 (2009) 6921–6928.
[60] J.A. Rodriguez, T. Jirsak, J. Dvorak, S. Sambasivan, D. Fischer, J. Phys. Chem. B 104 (2000) 319–328.
[61] X. Wang, H.Y. Chen, W.M.H Sachtler, J. Catal. 197 (2001) 281–291.
[62] A. Rahman, M. Ahmed, Stud. Surf. Sci. Catal. 100 (1996) 419–426.
[63] T. Yamaguchi, N. Ikeda, H. Hattori, K. Tanabe, J. Catal. 67 (1981) 324–330.
[64] N. Tang, Y. Liu, H.Q. Wang, Z.B. Wu, J. Phys. Chem. C 115 (2011) 8214–8220.
[65] B.X. Shen, Y.Y. Wang, F.M. Wang, T. Liu, Chem. Eng. J. 236 (2014) 171–180.
[66] B.X. Shen, X.P. Zhang, H.Q. Ma, Y. Yao, T. Liu, J. Environ. Sci. 25 (2013) 791–800.
[67] K. Nakamoto, Infrared and Raman Spectra of Inorganic and Coordination Compounds, fourth ed., Wiley, New York, NY, 1986.
[68] L. Li, Z.M. Chen, J. Ding, Spectrosc. Spectral Anal. 24 (2004) 1556–1559.
[69] J.H. Huang, Z.Q. Tong, Y. Huang, J.F. Zhang, Appl. Catal., B: Environ. 78 (2008) 309–314.